Electrochemical synthesis of sulfur-doped iron oxide in aqueous ferrous sulfate solution

Yusheng Yang[1] (iD), Shuyan Zhang[1], Tuoyao Wang[2], Ran Zhao[1], and Zengwu Zhao[1,3,*]

[1] *Key Laboratory of Integrated Exploitation of Bayan Obo Multi-Metal Resources, School of Material and Metallurgy, Inner Mongolia University of Science and Technology, Baotou 014010, China*
[2] *School of Energy & Environment, Inner Mongolia University of Science and Technology, Baotou 014010, China*
[3] *Collaborative Innovation Center of Integrated Exploitation of Bayan Obo Multi-Metal Resources, Inner Mongolia University of Science and Technology, Baotou 014010, China*

ABSTRACT

Energy storage devices and conversion systems have attracted more and more attention with the rapid development of clean energy. Iron oxide is widely used as electrode materials and electrocatalysts because of its abundant resource, low cost, and superior electrical and catalytic properties. Doping sulfur in iron oxide is an effective method to improve electrochemical and photocatalytic performance. The common synthesis method of sulfur-doped iron oxide is a three-step method of co-precipitation, hydrothermal, and calcination. This method has to be performed under high pressure and high temperature, so it needs to consume more energy. In this work, the electrochemical synthesis of sulfur-doped iron oxide was investigated under atmospheric pressure and temperature in the aqueous ferrous sulfate solution that was used as the precursors of sulfur, iron and oxygen. The influences of solution pH on the electrochemical synthesis process and the composition and morphology of deposits were investigated by the analyses of electrochemical reaction and SEM–EDS of deposits. It was found that the oxygen content in the deposit decreased as the pH value of the solution increased. There were three electrochemical reduction processes in sequence from positive to negative potential, followed by the underpotential deposition of iron on the platinum electrode, hydrogen evolution and sulfur doping. The sheet sulfur-doped iron oxide was successfully prepared by electrodeposition under a potential more negative than -1.70 V vs MSE. The kinetics of the electrochemical reaction of iron ions on the platinum electrode was investigated. The reduction process was a quasi-reversible process controlled by diffusion. The heterogeneous charge transfer rate constant k_s and the diffusion coefficient D were obtained.

Address correspondence to E-mail: zhzengwu@imust.edu.cn

1 Introduction

More clean energies such as wind and solar energy have been used for power generation to reduce thermal power generation and global greenhouse gas emissions. With the development of clean energies, energy storage devices and conversion systems have also received more and more attention. Transition metal oxides are widely used as electrode materials and electrocatalysts because of their abundant resources, low cost, and superior electrical and catalytic properties [1–4].

Iron oxides have been considered as a promising anode material for rechargeable batteries and photocatalytic materials [5–9]. However, the application of iron oxide to electrode materials was limited due to the poor rate capability [10]. And the application prospect of iron oxide as a photocatalytic material was also affected due to the low diffusion length (2–4 nm) and high electron–hole recombination rate [11]. To address the aforementioned limitations, many efforts have been made including construction of heterojunction, introduction of oxygen vacancies, nanostructuring and elemental doping [12–14]. Currently, anion doping in iron oxides is a straightforward and cost-effective strategy to enhance the electrochemical and photocatalytic properties [15–19].

According to the first principle calculations, the doping of sulfur can reduce the band gap of iron oxides from 2.34 to 1.18 eV and thus improve electronic conductivity [10].It has been reported that the conductivity of sulfides was nearly 100 times higher than oxides [20–22]. And it was found that the doping of sulfur in the metal oxide can minimize the charge transfer resistance, thereby improving the electrochemical performance [1]. In addition, sulfur is considered to be ideal dopant to improve the photochemical performance because of its low electronegativity. It was reported that the photocatalytic performance of α-Fe_2O_3 for carbamazepine degradation [23] was remarkably enhanced after doping with sulfur. The sulfur-doped α-Fe_2O_3 electrode showed a very high capacity of 0.81 mAh/cm^2 at 4 mA/cm^2. Guo et al. also reported that sulfur-doped iron oxide can promotes the photo-Fenton reaction and enhance removal of acid orange 7 and phenol [24].

Although there were some differences in the sulfur precursor and the reaction temperature in the synthesis process, sulfur-doped iron oxide are synthesized usually through a three-step method, including co-precipitation, hydrothermal and calcination processes [1, 23–25]. For example, Huang et al. used lipoic acid as the precursor of sulfur dopant atoms to prepare sulfur-doped iron oxide at 923 K [26]. Sulfur-doped iron oxide was synthesized using ferrous sulfate and $Na_2S_2O_3$ in the literature [24]. In these synthesis processes, high pressure and high temperature were used. To reduce greenhouse gas emissions, a technology that can be implemented under atmospheric pressure and temperature should be developed. Electrochemical methods are promising in synthesis with the development of clean electrical power.

In this work, the electrochemical synthesis of sulfur-doped iron oxide was investigated under atmospheric pressure and temperature. The aqueous ferrous sulfate solution was used as the precursors of sulfur, iron and oxygen. The feasibility of directly preparing sulfur-doped iron oxide through electrochemical reaction was studied in the ferrous sulfate solution. The influence of solution pH on the electrochemical reduction process was studied by combining the analyses of electrochemical reaction and SEM–EDS of deposits. The kinetics of the electrochemical reaction was also discussed in this work.

2 Experimental section

Iron sulfate heptahydrate (99.95% metals basis, CAS No. 7782–63-0) was sourced from Aladdin Industrial Corporation. A borosilicate glass cell of diameter 50 mm and height 66 mm was used for electrochemical experiments. The electrolytic cell was heated by a water bath to maintain the devised temperature ($\pm$ 0.1 K). The iron sulfate heptahydrate was dissolved in deionized water as electrolyte and the volume of electrolyte was kept constant at 30 ml. The concentration of ferrous sulfate was adjusted to 1.43 mol/l, which was close to saturation at 298.15 K. The pH value of electrolyte was adjusted by adding sulfuric acid, and measured by a pH electrode (LE438, Mettler Toledo) and a pH meter (SP-2100, Suntex, $\pm$ 0.01 pH). The pH electrode was calibrated in standard solutions with pH 4, 7 and 10.

All electrochemical researches were carried out through Autolab electrochemical workstation (PGSTAT 302 N, Metrohm) in a standard three electrode cell. Bright platinum wire (d = 1.0 mm, 99.95%

purity) and platinum gauze (99.95% purity) were used as working electrode and counter electrode, respectively. A mercurous sulfate electrode (MSE, ALS Co., Ltd) served as standard reference electrode (E^0 = 657 mV vs RHE at 298.15 K). The potentials given in this work were relative to MSE reference electrode. The deposits were prepared by potentiostatic electrolysis on a platinum disk electrode and their morphologies were observed by scanning electron microscope (SEM, Supra 55VP, Zeiss).

3 Results and discussion

3.1 Thermodynamic analysis of electrodeposition of iron

Figure 1 shows Pourbaix diagrams calculated by Factsage 8.0 software (customer ID: 0473) in the aqueous solution (Fig. 1a) and sulfate solution (Fig. 1b), respectively. As seen from the Pourbaix diagrams, the phase of iron oxides becomes more stable as the pH value of the solution increases at a constant potential. In addition, iron ions can be reduced to metallic iron at a more negative potential than −0.40 V vs SHE in the aqueous solution, but only FeS_2 in the sulfate solution. There is no relevant data of sulfur-doped iron oxide in the software database.

It was reported that the iron composition of deposits increased with increasing pH in sulfuric acid [27], hydrofluoric acid [28] and citric acid solution [29]. In order to prepare sulfur-doped iron oxide, it

was considered that iron oxide should be firstly deposited on the electrode surface, and then sulfur could be doped into iron oxide at a more negative potential. Iron oxide is easier to be formed in a solution with higher pH as seen from Fig. 1. And the doping of sulfur is easier at a more negative potential. Therefore, the influence of solution pH and reduction potential on the electrochemical preparation of sulfur-doped iron oxide has to be considered in this work.

3.2 Voltammetry in the ferrous sulfate solution with pH 1 and 4

According to the Pourbaix diagrams in Fig. 1 and the report in the literature [27], the oxygen content was dependent on the pH value of the solution. The ratio of oxygen to iron increased as the pH value of the solution decreased. Therefore in this work, the ferrous sulfate solutions with pH 1 and 4 were used as electrolytes to investigate the effect of the pH value of the solution on the electrochemical reduction process.

Figure 2 shows cyclic voltammograms in the ferrous sulfate solution with pH 4 on a Pt electrode. When the potential was limited to −0.70 V, a pair of redox peaks R1/O1 can be observed from the cyclic voltammogram. Since hydrogen has not yet formed at the R1 potential based on the Pourbaix diagrams in Fig. 1, the reaction at R1 should correspond to the reduction process of Fe(II) ions. According to the reports in the literatures [27, 28], a solid solution of platinum with some iron can be formed by
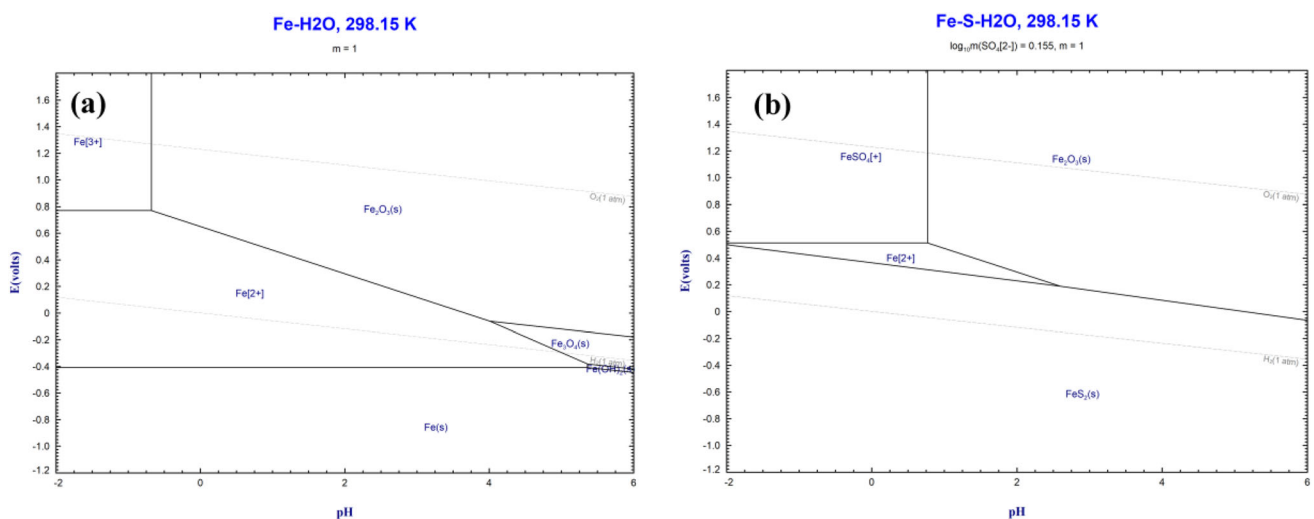

Fig. 1 Pourbaix diagrams calculated by Factsage 8.0 software in **a** aqueous solution and **b** sulfate solution with 1.43 mol/l at 298.15 K
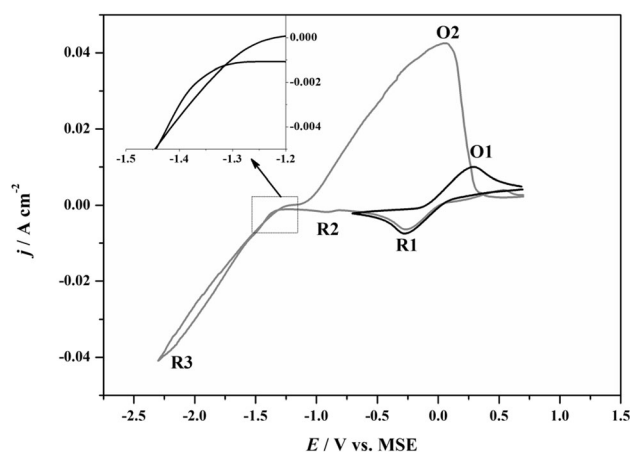
Fig. 2 Cyclic voltammograms in the ferrous sulfate solution with 1.43 mol/l with pH 4 at 298.15 K. Working electrode: bright Pt wire; reference electrode: MSE; counter electrode: platinum gauze; sweep rate: 0.10 V/s

Fig. 3 Cyclic voltammograms in the ferrous sulfate solution (1.43 mol/l) with pH 1 at 298.15 K. Working electrode: bright Pt wire; reference electrode: MSE; counter electrode: platinum gauze; sweep rate: 0.10 V/s

underpotential deposition and the formed solid solution at this potential contained a lot of oxygen. Therefore, this reaction process R1 is considered to be the underpotential deposition of Fe(II) ions on the platinum electrode.

When applying more cathodic potential, two new reduction signals R2 and R3 were observed on the CV curve. In addition, a "crossover" of the curve around −1.30 V was observed, which is more obvious on the magnified image. The formation of R2 peak was due to the evolution of hydrogen. The "crossover" was also found on the CV curve in LiCl–KCl-DyCl$_3$ melts and called as the "nucleation crossover effect", indicating the formation of stable nuclei on the electrode [30]. In this solution, the reaction process at R3 could be the formation of metallic iron or FeS$_2$. The electrochemical reactions are further studied by combining the composition of deposits. Moreover, there was only one oxidation peak O2 on the CV curve, and the oxidation peak O1 was gone. The reaction at O2 should correspond to the dissolution of deposits on the electrode surface. The oxidation signal O1 disappeared because the solid solution of platinum and iron was consumed by further reduction at a more negative potential.

Figure 3 shows cyclic voltammograms of the ferrous sulfate solution at pH 1 on a Pt electrode. It can be found that the redox processes of ions in the solution at pH 1 are significantly different from those in the solution at pH 4. A reduction peak R1 was observed from cyclic voltammogram as the sweep
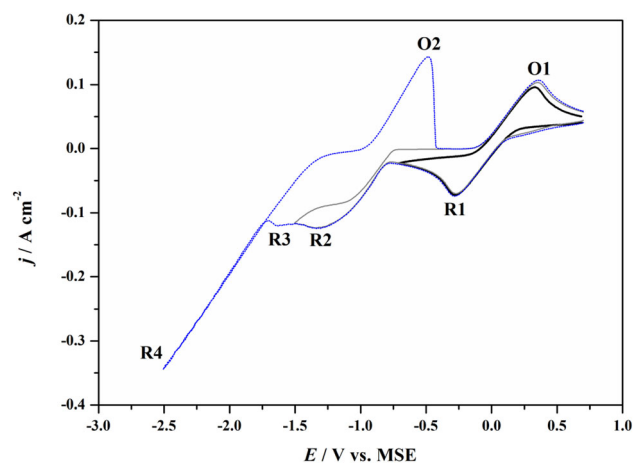
potential was limited to −0.70 V. This reduction process should correspond to the formation of the Pt-Fe solid solution, which is consistent with the result in Fig. 2. However, the oxidation peak O1 was still observed when the sweep potential was limited to −1.50 and −2.50 V. This indicates that the formed Pt-Fe solid solution was stable at a more negative potential.

The reduction process R2 was observed from CV curve as the sweep potential was limited to −1.50 V, but the corresponding oxidation peak was not. Since the formed hydrogen escaped, the oxidation process of hydrogen cannot be detected on the surface of the electrode. This indicates the peak R2 corresponds to the formation of hydrogen. When the sweep potential was limited to −2.50 V, the reduction processes R3/R4 and the corresponding oxidation peak O2 were observed from CV curve. The electrochemical reactions are further studied by combining the composition of deposits. In addition, it can be found that the current densities of the reaction at R4 and the reaction of forming hydrogen in the ferrous sulfate solution with pH 1 are greater than those in the ferrous sulfate solution with pH 4 by comparing CVs in Figs. 2 and 3. Since the current density is usually proportional to the reaction rate, the deposit and hydrogen can be prepared more quickly in the ferrous sulfate solution at pH 1.

Figure 4 shows linear sweep voltammograms in the ferrous sulfate solution at pH 1 and pH 4. The potentials of Fe(II) on the platinum electrode are very
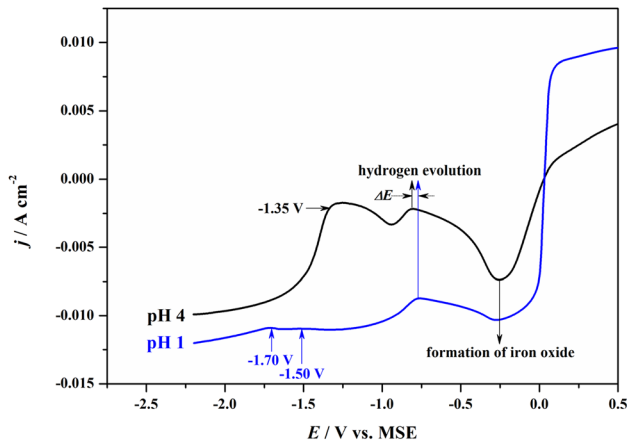
Fig. 4 Linear sweep voltammograms in the ferrous sulfate solution with 1.43 mol/l at pH 1 and pH 4 at 298.15 K. Working electrode: bright Pt wire; reference electrode: MSE; counter electrode: platinum gauze; sweep rate: 1 mV/s

close as seen from curves, indicating that the pH value of ferrous sulfate solution hardly affects the formation potential of the Pt-Fe solid solution. However, the pH value of ferrous sulfate solution affects the potential of hydrogen evolution. The reduction potential of hydrogen ions is more positive in a solution with lower pH. In addition of the two reactions, the reduction process at a more negative potential in these two solutions is different. The two processes at −1.50 and −1.70 V in the ferrous sulfate solution with pH 1 correspond to the reactions at R3 and R4 in Fig. 3, respectively. The reaction potential in the ferrous sulfate solution with pH 4 is more positive than that in the ferrous sulfate solution with pH 1. Moreover, the current densities for these reactions in the ferrous sulfate solution with pH 1 are greater than those in the ferrous sulfate solution with pH 4. This is consistent with the results of CVs in Figs. 2 and 3.

3.3 Compositions and morphologies of deposits obtained by potentiostatic electrolysis

In order to further understand these electrochemical reactions in the ferrous sulfate solution with pH 1 and pH 4, potentiostatic electrolysis was applied to obtain deposits on a platinum disk electrode. Figure 5 shows SEM images and EDS analyses of deposits after electrodeposition at −0.50 V for 10 min in the ferrous sulfate solution at pH 1 and pH 4. At

this applied potential, the deposits reduced at R1 in Figs. 2 and 3 can be prepared.

As seen from the Fig. 5a, some cotton-like deposits were formed on the surface of the platinum electrode in the ferrous sulfate solution at pH 1. These deposits are composed of Pt, O and Fe based on the EDS analysis in Fig. 5b, indicating the reaction corresponds to the formation of the solid solution of Pt with some Fe. And iron oxide is the main form of iron at such a reduction potential, which is consistent with the report [27]. Comparing with the result calculated by Factsage software in Fig. 1a, the reduction potential of iron on the platinum electrode is more positive than the theoretical potential, indicating platinum has a depolarizing effect on iron.

Many cotton-like deposits are seen from the Fig. 5c on the surface of the platinum electrode in the ferrous sulfate solution at pH 4. The composition and morphology of deposits are very similar to that in the ferrous sulfate solution at pH 1. According to the results of Fig. 5, iron containing oxygen can be pre-deposited on the platinum electrode surface in both solutions. In other words, there is a possibility of preparing sulfur-doped iron oxide in both solutions.

A more negative potential was applied to obtain deposits in the ferrous sulfate solution at pH 4. Figure 6a and b shows SEM images of deposits after electrodeposition at −1.80 V for 10 min. As seen from SEM images with different magnifications, the surface of the platinum disk electrode has been completely covered by deposits. The deposits are composed of many particles with a particle size of around 1 μm. These particles are very pure metallic iron and no sulfur was doped into the deposits based on the EDS analysis in Fig. 6c. Therefore, it demonstrates that the reduction process at R3 in Fig. 2 is the electrodeposition of metallic iron. However, there is no oxygen in the deposits under such a negative reduction potential.

According to the results of CV, LSV, and SEM–EDS analyses, the electrochemical reduction process is proposed in the ferrous sulfate solution at pH 4. Fe(II) ions are first reduced and then deposited on the surface of the platinum electrode to form Pt-Fe solid solution. The reduction peak potential of this reaction is about −0.25 V. There is a lot of oxygen in the deposits because of the positive reduction potential. As the reduction potential becomes more negative, hydrogen is formed on the surface of the electrode at −0.80 V. In this process, the iron content on the
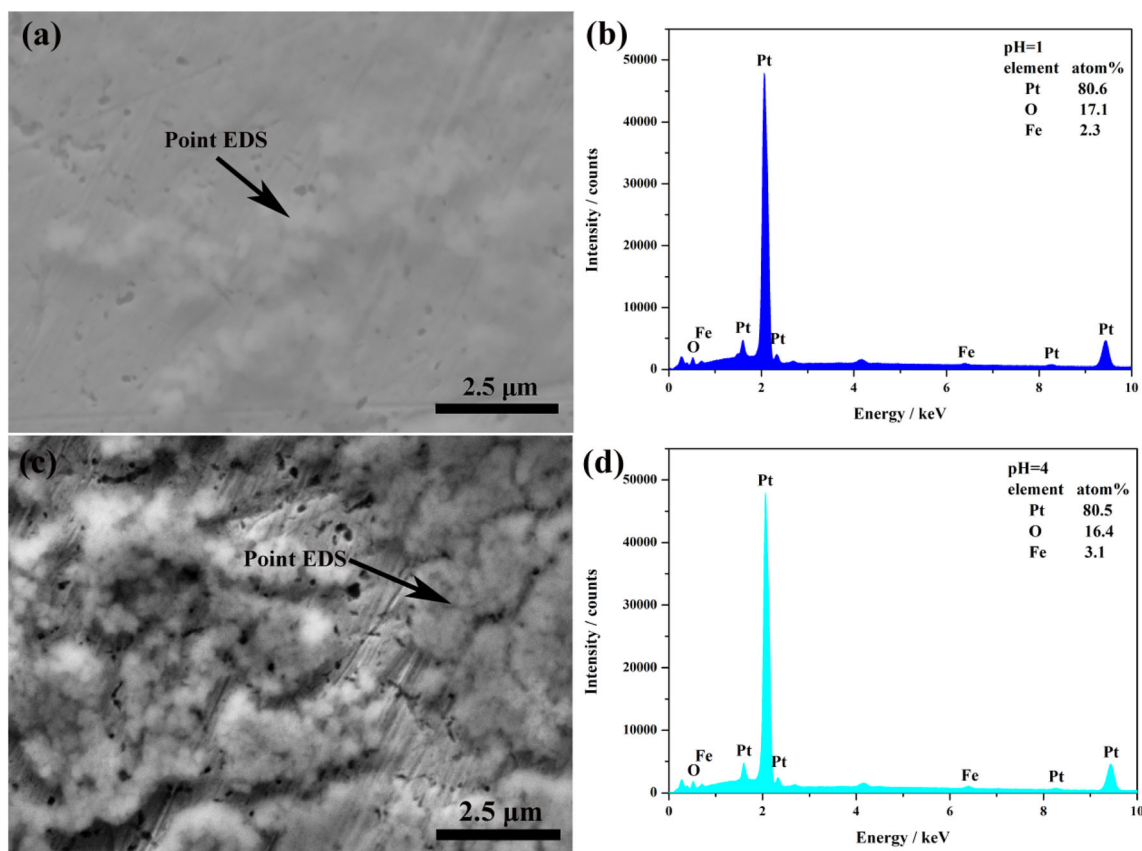
Fig. 5 SEM images and EDS analyses of deposits on a platinum disk electrode after electrodeposition at −0.50 V vs MSE for 10 min in the ferrous sulfate solution (1.43 mol/l) with (**a**, **b**) pH 1 and (**c**, **d**) pH 4 at 298.15 K
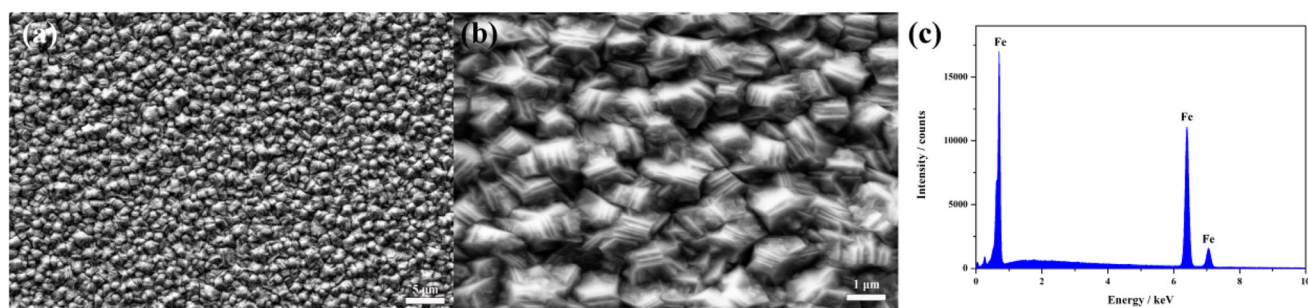

Fig. 6 **a** and **b** SEM images of deposits on a platinum disk electrode with different magnifications after electrodeposition at −1.80 V vs MSE for 10 min in the ferrous sulfate solution (1.43 mol/l) with pH 4 at 298.15 K; **c** EDS analysis of electrode surface

electrode surface increases and the oxygen content decreases. When the reduction potential is more negative than −1.35 V, pure iron is formed on the cathodic surface. In the ferrous sulfate solution at pH 4, sulfur is not doped into the deposits.

Figure 7a shows SEM image of deposits after electrodeposition at −1.80 V for 10 min in the ferrous sulfate solution at pH 1. Some sheet deposits are observed from the SEM image. These deposits are composed of Fe, O and S based on the EDS mapping analysis. The compositions of the sheet and the platinum electrode surface under the sheet were analyzed by EDS. The result indicates that the sheet is sulfur-doped iron oxide. And the deposits on the platinum electrode surface are composed of iron, platinum, oxygen and little sulfur. The composition of the deposit is similar to that obtained at −0.50 V, but it has higher iron content.
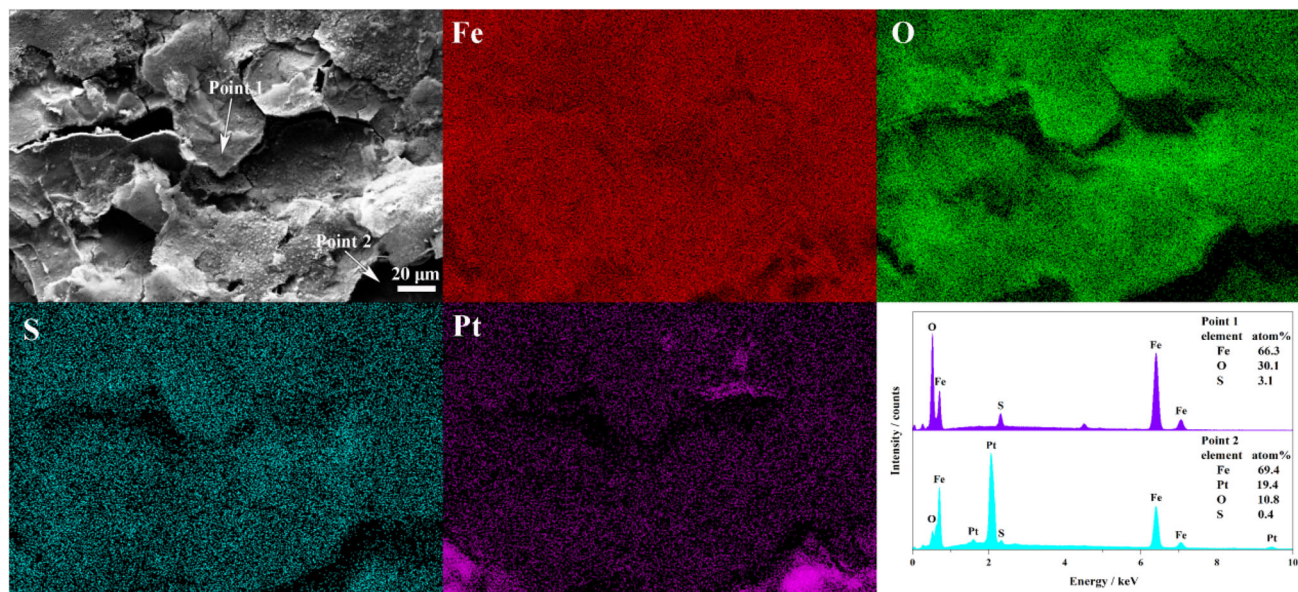
Fig. 7 SEM image and EDS analyses of deposits on a platinum disk electrode after electrodeposition at −1.80 V vs MSE for 10 min in the ferrous sulfate solution (1.43 mol/l) with pH 1 at 298.15 K

According to the results of CV, LSV, and SEM–EDS analyses, the electrochemical reduction process is proposed in the ferrous sulfate solution at pH 1. The formation of Pt-Fe solid solution and the reduction of hydrogen in the ferrous sulfate solution at pH 1 are same as those in the ferrous sulfate solution at pH 4, except that the reduction potential (about −0.75 V) of hydrogen ions in the ferrous sulfate solution at pH 1 is more positive. However as the potential becomes more negative, the oxygen on the electrode surface is not completely reduced due to the stronger acidity of the solution. Finally, sulfur elements are successfully doped into iron oxides at −1.70 V.

3.4 Kinetics of the reaction process of iron ions on the platinum electrode

According to the above results, the formed iron oxide on the platinum electrode is the precursor for the preparation of sulfur-doped iron oxide in the ferrous sulfate solution with pH 1. Therefore, the kinetics of the electrode process of iron ions on the platinum electrode was investigated.

Figure 8 shows cyclic voltammograms with various sweep rates at four temperatures on a platinum electrode. The redox peak potentials of Fe(II)/Fe(0) on a platinum electrode shift significantly as the sweep rate increases from 20 to 400 mV/s. The difference between the anodic peak potential (E_{pa}) and

the cathodic peak potential (E_{pc}) for a reversible process is not greater than 58 mV at 298 K [31]. Therefore, the processes in Fig. 8 are not reversible because the potential differences are much greater than 58 mV at 298 K.

Table 1 shows the peak parameters and kinetic parameters obtained from Fig. 8. The values of $1/2(E_{pc} + E_{pa})$ at same temperature are almost constant for all sweep rates, suggesting that the reaction processes should be quasi-reversible processes [32]. The heterogeneous charge transfer rate constant (k_s) is an important criterion for reversibility. Perone [33], Nicholson [34] and Klingler-Kochi [35] proposed the calculation methods of the heterogeneous charge transfer rate constant. The methods proposed Perone [33] and Nicholson [34] are not applicable in this work because of the limitation of the potential difference ($E_{pc}-E_{pa}$). Therefore, the heterogeneous charge transfer rate constant was calculated by Eq. (1) [35].

$$k_s = 2.18\left[\frac{D\alpha n vF}{RT}\right]^{1/2} \exp\left[\frac{\alpha^2 nF}{RT}\left(E_{pc} - E_{pa}\right)\right] \quad (1)$$

In the Eq. (1), α is the charge transfer coefficient, D is the diffusion coefficient (cm^2/s), v is the scan rate (V/s), k_s is the heterogeneous charge transfer rate constant (cm/s), F is the Faraday constant (C/mol), n is the number of electrons involved in the charge transfer reaction, T is the reaction temperature (K)
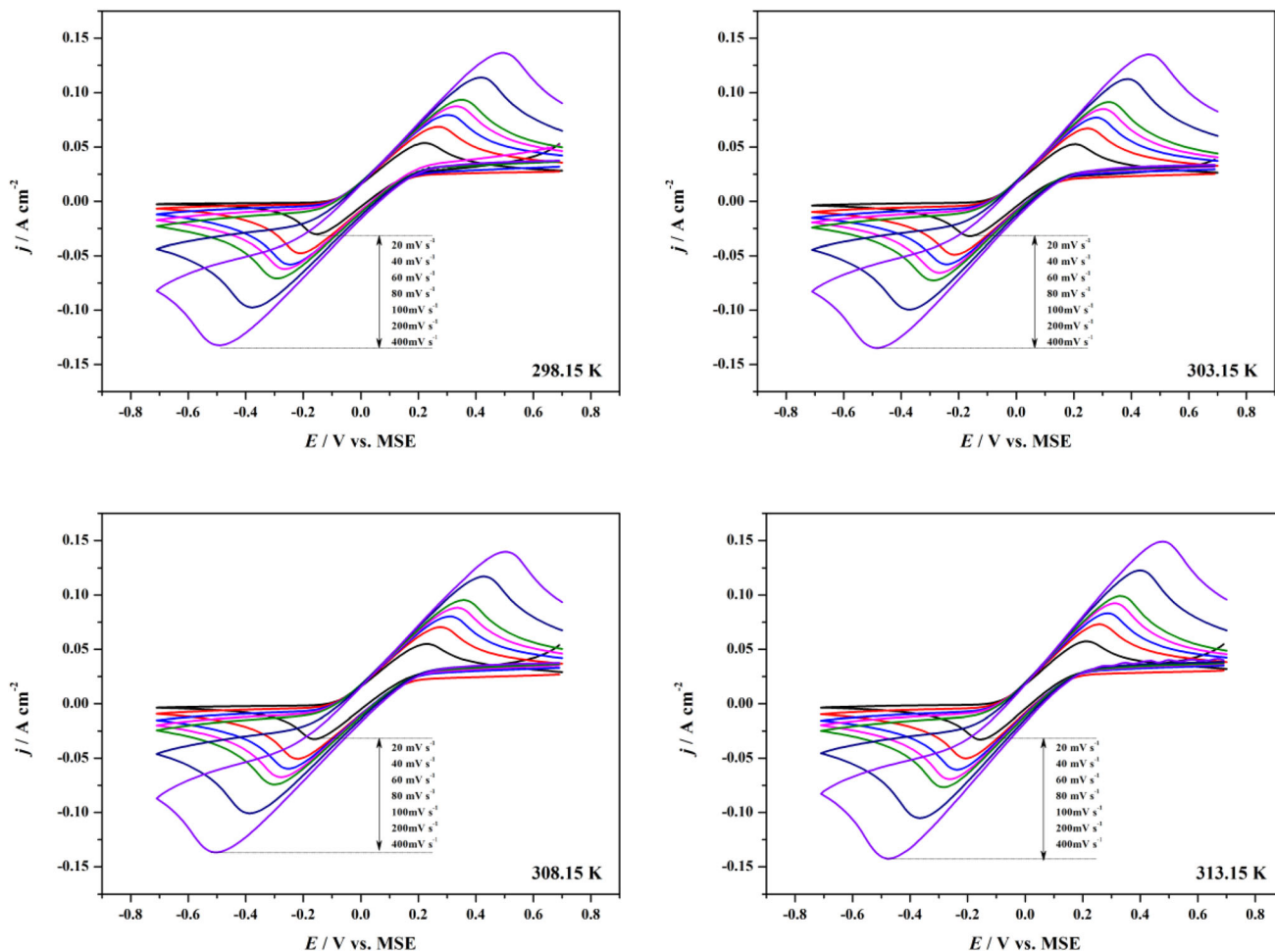
Fig. 8 Cyclic voltammograms in the ferrous sulfate solution (1.43 mol/l) with pH 1 for different scan rates at four temperatures. Working electrode: bright Pt wire; reference electrode: MSE; counter electrode: platinum gauze

and R is the ideal gas constant (J/mol/K). The charge transfer coefficient α can be calculated by the Eq. (2) [31].

$$\left|E_{pc} - E_{p/2}\right| = \frac{1.857RT}{\alpha nF} \quad (2)$$

where $E_{p/2}$ is the half-peak potential (V). The diffusion coefficient D can be obtained by Eq. (3) [31] where c_0 is the bulk concentration of electro-active species (mol/cm^3) and j_{pc} is the cathodic peak current density (A/cm^2).

$$j_{pc} = 0.496nFc_0\left(\frac{\alpha nFvD}{RT}\right)^{1/2} \quad (3)$$

Figure 9 shows the relationship of j_{pc} and $v^{1/2}$, where the data were plotted and linearly fitted. Four fitting lines do not pass through the origin, indicating that the reduction process of Fe(II) on the platinum

electrode is neither reversible nor irreversible, and is controlled by diffusion.

The diffusion coefficient and the heterogeneous charge transfer rate constant were calculated and their results are listed in Table 1. The diffusion coefficient of iron ions in the ferrous sulfate solution is an order of magnitude from that calculated in the hydrofluoric acid solution in our previous work [28]. However, it can be found that the diffusion coefficient and the heterogeneous charge transfer rate constant in the ferrous sulfate solution are faster than those in the hydrofluoric acid solution.

According to the criterion for reversibility [31], the process is irreversible if $3.7 \times 10^{-6} >$ the value of ($k_s/v^{1/2}$). The process is a quasi-reversible process if $0.11 >$ the value of ($k_s/v^{1/2}$) $> 3.7 \times 10^{-6}$. If the value of ($k_s/v^{1/2}$) > 0.11, it is a reversible process. Therefore, the reaction process of Fe(II) on the platinum

Table 1 Peak parameters obtained from Fig. 8 and the kinetic parameters at four temperatures

T/K	v/V/s	E_{pc} / V	E_{pa}/V	½ ($E_{pc} + E_{pa}$)/V	j_{pc}/A/cm^2	$D \times 10^{-7}$/cm^2/s	$k_s \times 10^{-4}$/cm/s	$k_s/v^{1/2}$
298.15	0.02	−0.156	0.227	0.036	−0.030	2.26	2.66	0.0019
	0.04	−0.206	0.267	0.030	−0.048	3.13	4.20	0.0021
	0.06	−0.247	0.307	0.030	−0.058	3.58	5.52	0.0022
	0.08	−0.267	0.338	0.036	−0.062	3.22	5.92	0.0021
	0.1	−0.287	0.348	0.030	−0.071	3.48	6.86	0.0022
	0.2	−0.378	0.418	0.020	−0.098	4.27	10.69	0.0024
	0.4	−0.488	0.489	0	−0.132	4.69	15.27	0.0024
303.15	0.02	−0.156	0.207	0.026	−0.032	2.37	2.78	0.0020
	0.04	−0.216	0.247	0.016	−0.049	3.32	4.47	0.0022
	0.06	−0.247	0.277	0.015	−0.058	3.40	5.49	0.0022
	0.08	−0.267	0.307	0.020	−0.066	3.42	6.22	0.0022
	0.1	−0.287	0.338	0.026	−0.073	3.51	6.91	0.0022
	0.2	−0.367	0.388	0.010	−0.099	4.00	10.40	0.0023
	0.4	−0.488	0.458	−0.015	−0.138	4.80	15.65	0.0025
308.15	0.02	−0.166	0.227	0.030	−0.032	2.75	2.97	0.0021
	0.04	−0.216	0.277	0.030	−0.051	3.71	4.58	0.0023
	0.06	−0.247	0.307	0.030	−0.060	3.78	5.63	0.0023
	0.08	−0.277	0.338	0.030	−0.068	3.96	6.64	0.0024
	0.1	−0.297	0.357	0.030	−0.074	4.00	7.32	0.0023
	0.2	−0.388	0.428	0.020	−0.101	4.41	10.60	0.0024
	0.4	−0.498	0.509	0.006	−0.137	4.60	14.61	0.0023
313.15	0.02	−0.156	0.217	0.030	−0.033	2.66	2.96	0.0021
	0.04	−0.206	0.257	0.026	−0.050	3.46	4.52	0.0023
	0.06	−0.236	0.287	0.026	−0.061	3.72	5.70	0.0023
	0.08	−0.267	0.317	0.025	−0.069	4.01	6.77	0.0024
	0.1	−0.287	0.328	0.020	−0.077	4.09	7.69	0.0024
	0.2	−0.367	0.398	0.016	−0.105	4.48	10.87	0.0024
	0.4	−0.478	0.478	0	−0.143	4.86	15.39	0.0024
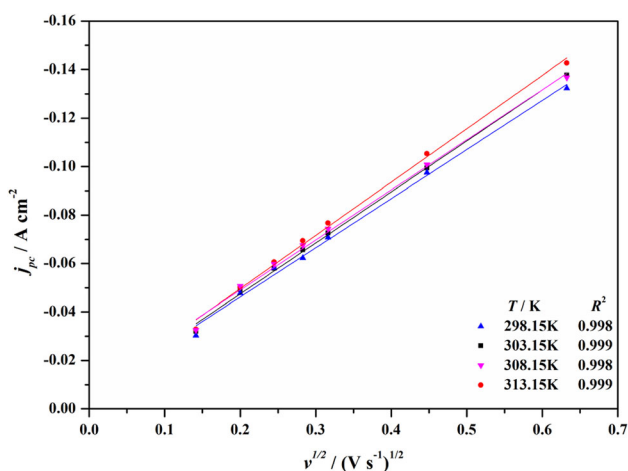
Fig. 9 Variation of peak current density versus the square root of potential sweep rate at four temperatures

electrode is a quasi-reversible process based on the results in Table 1.

4 Conclusions

The sulfur-doped iron oxide was successfully prepared by electrodeposition in aqueous ferrous sulfate solution. Three electrochemical reduction processes occurred in sequence from positive to negative potential, followed by the underpotential deposition of iron on the platinum electrode, hydrogen evolution and sulfur doping. Sulfur can be doped into the Pt-Fe solid solution containing oxygen under a potential more negative than −1.70 V vs MSE. The morphology of the sulfur-doped iron oxide obtained by electrodeposition is sheet.

The pH value of aqueous ferrous sulfate solution significantly affected the electrochemical reduction process. As the pH value of the solution increased, the oxygen content in the deposit on the platinum electrode decreased. It is difficult for sulfur to dope into the pure iron deposited at the cathode, but it can be doped into iron oxides. Therefore, it is suggested that sulfur replaced oxygen in iron oxides to form sulfur-doped iron oxide.

The kinetics of the electrochemical reaction of iron ions on the platinum electrode was investigated. The reduction process is a quasi-reversible process controlled by diffusion. The heterogeneous charge transfer rate constant k_s and the diffusion coefficient D were obtained.

Acknowledgements

Author contributions

YY: Writing—review & editing, Conceptualization, Formal Analysis, Funding acquisition, Investigation, Methodology, Writing original draft. SZ: Data curation, Investigation, Visualization, Software. TW: Investigation, Visualization. RZ: Investigation, Visualization. ZZ: Funding acquisition, Resources, Supervision. All authors read and approved the final manuscript.

Funding

Data availability

The datasets generated during and/or analysed during the current study are available from the corresponding author on reasonable request.

Declarations

Conflict of interest The authors have no relevant financial or non-financial interests to disclose.

References

1. S. Lalwani, A. Joshi, G. Singh, R.K. Sharma, Electrochim. Acta **328**, 135076 (2019)
2. A. Kargar, S. Yavuz, T.K. Kim, C.H. Liu, C. Kuru, C.S. Rustomji, S. Jin, P.R. Bandaru, ACS Appl. Mater. Interfaces. **7**, 17851 (2015)
3. L. Liu, H. Zhang, Y. Mu, Y. Bai, Y. Wang, J. Power Sources. **327**, 599 (2016)
4. S. Lalwani, R.B. Marichi, M. Mishra, G. Gupta, G. Singh, R.K. Sharma, Electrochim. Acta. **283**, 708 (2018)
5. Y. Wang, H. Wei, H. Lv, Z. Chen, J. Zhang, X. Yan, L. Lee, Z.M. Wang, Y.L. Chueh, ACS Nano **13**, 11235 (2019)
6. Y. Wang, Z. Chen, T. Lei, Y. Ai, Z. Peng, X. Yan, H. Li, J. Zhang, Z.M. Wang, Y.L. Chueh, Adv. Energy Mater. **8**, 1703453 (2018)
7. J. Liu, M. Chen, L. Zhang, J. Jiang, J. Yan, Y. Huang, J. Lin, H.J. Fan, Z.X. Shen, Nano Lett. **14**, 7180 (2014)
8. D. Lei, D.C. Lee, E. Zhao, A. Magasinski, H.R. Jung, G. Berdichevsky, D. Steingart, G. Yushin, Nano Energy **48**, 170 (2018)
9. C. Guo, C. Li, Nano Energy **42**, 166 (2017)
10. J. Yang, Q. Zhang, Z. Wang, Z. Wang, L. Kang, M. Qi, M. Chen, W. Liu, W. Gong, W. Lu, P.P. Shum, L. Wei, Adv. Energy Mater. **10**, 2001064 (2020)
11. M. Mishra, D.M. Chun, Appl. Catal. A: Gen. **498**, 126 (2015)
12. Y. Zhang, S. Jiang, W. Song, P. Zhou, H. Ji, W. Ma, W. Hao, C. Chen, J. Zhao, Energy Environ. Sci. **8**, 1231 (2015)
13. H.J. Ahn, K.Y. Yoon, M.J. Kwak, J.H. Jang, Angew. Chem. Int. Ed. Engl. **55**, 9922 (2016)
14. Y. Zhou, M. Yan, J. Hou, Y. Niu, D. Ni, H. Shen, P. Niu, Y. Ma, Sol. Energy **179**, 99 (2019)
15. M. Yu, X. Cheng, Y. Zeng, Z. Wang, Y. Tong, X. Lu, S. Yang, Angew. Chem. Int. Ed. **55**, 6762 (2016)
16. L. An, J. Feng, Y. Zhang, R. Wang, H. Liu, G.C. Wang, F. Cheng, P. Xi, Adv. Funct. Mater. **29**, 1805298 (2019)
17. Z. Wang, H. Liu, R. Ge, X. Ren, J. Ren, D. Yang, L. Zhang, X. Sun, ACS Catal. **8**, 2236 (2018)

18. A.M. Elshahawy, C. Guan, X. Li, H. Zhang, Y. Hu, H. Wu, S.J. Pennycook, J. Wang, Nano Energy **39**, 162 (2017)

19. W. Xu, J. Chen, M. Yu, Y. Zeng, Y. Long, X. Lu, Y. Tong, J. Mater. Chem. A **4**, 10779 (2016)

20. W. Du, Z. Wang, Z. Zhu, S. Hu, X. Zhu, Y. Shi, H. Pang, X. Qian, J. Mater. Chem. A. **2**, 9613 (2014)

21. Y. Li, L. Cao, L. Qiao, M. Zhou, Y. Yang, P. Xiao, Y. Zhang, J. Mater. Chem. A. **2**, 6540 (2014)

22. J. Xiao, L. Wan, S. Yang, F. Xiao, S. Wang, Nano Lett. **14**, 831 (2014)

23. J. Deng, C. Ye, A. Cai, L. Huai, S. Zhou, F. Dong, X. Li, X. Ma, Chem. Eng. J. **420**, 129863 (2021)

24. L. Guo, F. Chen, X. Fan, W. Cai, J. Zhang, Appl. Catal. B-Environ. **96**, 162 (2010)

25. J. Du, J. Bao, X. Fu, H. Lu, S.H. Kim, Appl. Catal. B-Environ. **184**, 132 (2016)

26. H. Huang, Y. Lin, S. Chang, C. Liu, K. Wang, H. Jhong, J. Lee, C. Wang, J. Mater. Chem. A **5**, 19790 (2017)

27. K. Leistner, S. Oswald, J. Thomas, S. Fähler, H. Schlörb, L. Schultz, Electrochim. Acta **52**, 194 (2006)

28. Y. Yang, C. Lan, Y. Wang, Z. Zhao, B. Li, Sep. Purif. Technol. **230**, 115870 (2020)

29. T. Yanai, K. Furutani, T. Masaki, T. Ohgai, M. Nakano, H. Fukunaga, AIP Adv. **6**, 056014 (2016)

30. Y. Castrillejo, M.R. Bermejo, A.I. Barrado, R. Pardo, E. Barrado, A.M. Martínez, Electrochim. Acta **50**, 2047 (2005)

31. A.J. Bard, L.R. Faulkner, *Electrochemical methods: fundamental and applications* (Wiley, New York, 2001)

32. S. Mishra, K. Sini, Ch.J. Rao, C. Mallika, U.K. Mudali, Electroanal. Chem. **776**, 127 (2016)

33. S.P. Perone, Anal. Chem. **38**, 1158 (1966)

34. R.S. Nicholson, Anal. Chem. **37**, 1351 (1965)

35. R.J. Klingler, J.K. Kochi, J. Phys. Chem. **85**, 1741 (1981)